

Article

Impact of Bentonite Clay on In Situ Pyrolysis vs. Hydrothermal Carbonization of Avocado Pit Biomass

Madeline Karod ¹, Zoe A. Pollard ¹, Maisha T. Ahmad ¹, Guolan Dou ^{2,3}, Lihui Gao ⁴ and Jillian L. Goldfarb ^{1,*}

¹ Department of Biological and Environmental Engineering, Cornell University, Ithaca, NY 14853, USA; mk2574@cornell.edu (M.K.); zp84@cornell.edu (Z.A.P.); mta55@cornell.edu (M.T.A.)

² School of Safety Engineering, China University of Mining and Technology, Xuzhou 221116, China; gldou@cumt.edu.cn

³ Key Laboratory of Gas and Fire Control for Coal Mines, China University of Mining and Technology, Xuzhou 221116, China

⁴ School of Environmental Science and Spatial Informatics, China University of Mining and Technology, Xuzhou 221116, China; lihuigaocumt@163.com

* Correspondence: goldfarb@cornell.edu or jilliangoldfarb@gmail.com; Tel.: +1-(607)-255-5789

Abstract: Biofuels produced via thermochemical conversions of waste biomass could be sustainable alternatives to fossil fuels but currently require costly downstream upgrading to be used in existing infrastructure. In this work, we explore how a low-cost, abundant clay mineral, bentonite, could serve as an in situ heterogeneous catalyst for two different thermochemical conversion processes: pyrolysis and hydrothermal carbonization (HTC). Avocado pits were combined with 20 wt% bentonite clay and were pyrolyzed at 600 °C and hydrothermally carbonized at 250 °C, commonly used conditions across the literature. During pyrolysis, bentonite clay promoted Diels–Alder reactions that transformed furans to aromatic compounds, which decreased the bio-oil oxygen content and produced a fuel closer to being suitable for existing infrastructure. The HTC bio-oil without the clay catalyst contained 100% furans, mainly 5-methylfurfural, but in the presence of the clay, approximately 25% of the bio-oil was transformed to 2-methyl-2-cyclopentenone, thereby adding two hydrogen atoms and removing one oxygen. The use of clay in both processes decreased the relative oxygen content of the bio-oils. Proximate analysis of the resulting chars showed an increase in fixed carbon (FC) and a decrease in volatile matter (VM) with clay inclusion. By containing more FC, the HTC-derived char may be more stable than pyrolysis-derived char for environmental applications. The addition of bentonite clay to both processes did not produce significantly different bio-oil yields, such that by adding a clay catalyst, a more valuable bio-oil was produced without reducing the amount of bio-oil recovered.

Keywords: pyrolysis; hydrothermal carbonization; clay; catalyst; bio-oil upgrading



Citation: Karod, M.; Pollard, Z.A.; Ahmad, M.T.; Dou, G.; Gao, L.; Goldfarb, J.L. Impact of Bentonite Clay on In Situ Pyrolysis vs. Hydrothermal Carbonization of Avocado Pit Biomass. *Catalysts* **2022**, *12*, 655. <https://doi.org/10.3390/catal12060655>

Academic Editor: Tomás García

Received: 30 April 2022

Accepted: 8 June 2022

Published: 15 June 2022

Publisher's Note: MDPI stays neutral with regard to jurisdictional claims in published maps and institutional affiliations.



Copyright: © 2022 by the authors. Licensee MDPI, Basel, Switzerland. This article is an open access article distributed under the terms and conditions of the Creative Commons Attribution (CC BY) license (<https://creativecommons.org/licenses/by/4.0/>).

1. Introduction

The economic viability of a renewable-energy-based future depends on the ability to produce multiple high-value products from carbonaceous precursors including fuels, chemicals, and upgraded solid products. The health of the environment hinges on our ability to upcycle vast quantities of carbonaceous wastes that would otherwise decompose into greenhouse gases [1] into materials and fuels to establish a circular economy [2]. Thermochemical conversion techniques, such as pyrolysis and hydrothermal carbonization (HTC; also known as wet pyrolysis), can be used to produce bio-based fuels and platform chemicals as well as solid residues with myriad applications. However, the widespread implementation of such processes is hampered by the high oxygen content of the liquid products.

Pyrolysis and HTC bio-oils are heterogeneous (often containing upwards of 100 components) and require significant and often costly upgrading to improve issues surrounding

the stability, viscosity, and acidity of the fresh condensable biocrude [3–5]. The literature contains a vast knowledge of potential pyrolysis pathways and the impact of processing conditions (time, temperature, fixed vs. fluidized beds, feedstocks, etc.) on pyrolysis products [6]. Considerable work has been conducted on the downstream upgrading of such biofuels [7] and into the in situ upgrading (that is, the use of catalysts during pyrolysis and HTC) using preformed nanocatalysts and zeolites [8–10]. Attention has turned recently to the ability to in situ upgrade pyrolysis biofuels using a variety of clay minerals [11–15], whose (likely) cation exchange capacity promotes overall deoxygenation reactions including decarboxylation, decarbonylation, hydrogenolysis, and hydrodeoxygenation [16,17]. A small body of literature looks at the impact of including clay minerals during HTC of biomasses, sometimes couched in an investigation into clay transformation mechanisms [18]. A growing body of research demonstrates how in situ clay incorporation into hydrothermal processing can shift the oxygen and carbon ratios of the products, producing deoxygenated biocrudes as a result of the clays' Lewis acid and base sites [19–21]. Bentonite clay consists of metal oxides, mainly SiO_2 , Al_2O_3 , Fe_2O_3 , MgO , Na_2O , and K_2O , which provide Brønsted and Lewis acid centers within the clay [22]. Brønsted acid sites (i.e., proton donor sites) have been found to promote hydrocarbon yield in bio-oil, while Lewis acid sites (i.e., electron accepting sites) can catalyze decarboxylation by promoting the formation of radical groups [23]. For both pyrolysis and HTC, in situ upgrading schemes utilizing abundant and inexpensive clay minerals could reduce the cost of downstream upgrading and catalyst recovery, improving the economic viability of bio-oil production.

The valorization of solid carbonaceous residuals remaining from pyrolysis and HTC is a potential strategy to increase the economic viability of an integrated biorefinery [24]. Upgraded biochars and hydrochars are proposed for use in a variety of applications from water treatment to soil amendments to electrode materials [25–30]. Ramola et al. demonstrated that co-pyrolysis of bentonite and biomass composites impacts yield, surface texture, and the degree of carbonization, significantly increasing the surface area and adsorption capacity of the resulting heterogeneous biochars [31]. Likewise, montmorillonite (a primary component of the bentonite clay used in this work) has been shown to improve the nutrient retention of both biochars [32] and hydrochars [33] for potential use as soil amendments. Considerable work has been conducted to understand the impact of thermochemical processing parameters including temperature, residence time, and the biomass-to-water ratio (for HTC only), especially in terms of solid yield, carbon content, and higher heating values. However, there is scant research on the inclusion of clay minerals into the HTC process in order to produce upgraded solid materials; the available literature focuses on “pure” biomasses such as cellulose and starch [34,35].

In a previous study, we demonstrated how the incorporation of bentonite clay could be used to simultaneously in situ upgrade pyrolysis biofuels and produce a heterogeneous adsorbent using two biomasses: pineapple plant and mango pits [14]. Here, we extended this study by focusing on the impact of the bentonite clay during two conversion processes (i.e., pyrolysis and HTC) with a third biomass: avocado pits. The US avocado production was approximately USD 426 million in 2020 (latest available data), with over 200,000 tons produced among Florida and California [36]. Beyond domestic crop consumption, the US imports over USD 2.4 billion worth of avocados from Mexico annually. Since 1975, the Calavo Growers of California have run an avocado processing plant in Ventura County, CA, US, turning out more than 20 million pounds of avocado-based items a year, responsible for approximately 40% of worldwide commercial guacamole production [37]. Due to their high production and geographical concentration, avocado pits represent a viable feedstock for conversion.

By investigating the conversion of the same feedstock using the same clay catalyst via both pyrolysis and HTC, we can compare the quality of materials produced from a relatively high-energy process (pyrolysis) to materials produced at lower temperatures in a high-pressure environment that utilizes water as a solvent and catalyst [38]. The purpose of this was to determine which process would yield in situ upgraded biofuels with

lower oxygen contents and solid residuals with increased surface areas. This side-by-side comparison of pyrolysis and hydrothermal carbonization is one of few in the literature using the same biomass, in situ catalyst (during conversion), analytical techniques, and instrumentation for product analysis.

2. Results and Discussion

The two thermochemical conversion methods employed here—pyrolysis and hydrothermal carbonization (or wet pyrolysis)—are both touted as potential routes to produce both solid and liquid biofuels, in the forms of char and oil, respectively, from waste biomass. In this work, we compared the products (i.e., solid and liquid phases) generated through in situ catalyzed and uncatalyzed thermochemical conversion. Compounds were detected in the bio-oils and aqueous phase of the HTC using GC-MS and HPLC, respectively, to gauge the potential of the sample as a liquid fuel.

2.1. Bio-Oils and Biogas from Pyrolysis and Hydrothermal Carbonization

Product yields for pyrolysis and HTC for avocado pit and avocado pit + clay mixtures are provided in Figure 1. The liquid-phase yields did not differ significantly between in situ catalyzed and noncatalyzed pyrolysis, with a slightly lower liquid yield for clay-catalyzed HTC. The HTC liquid yield had a data range between 49.70 and 58.88, which is quite a large range for this process. The average of these two points was 54.29 as reported in Table S4. Avocado pits have previously been used as an HTC feedstock, and the average liquid yield was reported to be 54.11% for a reaction temperature of 240 °C and 50.39% for a reaction temperature of 250 °C [39]. The data reported in Figure 1 agree with these reports; small variations in the HTC reactor heating rate may explain the wide data range reported here. The condensable phase liquid bio-oil was 37–40 wt% for pyrolysis, and the liquid fraction for HTC was 41–54% (comprising both the aqueous process water and organic bio-crude). The resulting liquid phases were analyzed using GC-MS to determine their composition. Solid yields slightly increased (though not to a statistically significant degree) in both pyrolysis and HTC due to the incorporation of bentonite clay, an inorganic material that predominantly remains as a solid.

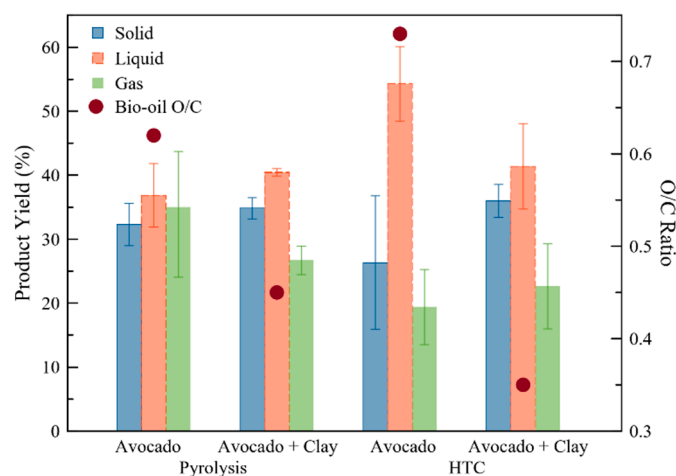


Figure 1. Yield of chars produced from pyrolysis and hydrothermal carbonization (average value is reported with one standard deviation about the mean).

Table 1 shows the compound species detected by GC-MS analysis in bio-oils produced during pyrolysis and hydrothermal carbonization for the biomass (i.e., avocado pits) and biomass + clay mixture. A complete list of individual compounds is presented in Table S1 of the online Supplemental Materials. Data are presented as the average of two data points and their range (where the two data points are the boundaries). From Tables 1 and S2, we can see that there were fewer compounds detected in the HTC bio-oil relative to

the pyrolysis bio-oil. As HTC occurs in an aqueous environment and produces a small fraction of bio-oil at 250 °C, it is likely that compounds formed during HTC via cellulose dehydration partition into the aqueous phase, as these are largely aqueous compounds [40]. Additionally, due to the instrument's constraints, compounds that elute very quickly (i.e., highly volatile compounds) are undetected by GC-MS. The water content of the bio-oils, both catalyzed and noncatalyzed, was determined (data reported in Table S3). For pyrolysis, the noncatalyzed bio-oil is approximately 2% water while the catalyzed bio-oil is 1% water. These values are statistically significantly different ($p < 0.05$, two-tailed t -test). The HTC bio-oil has an opposite trend, with the noncatalyzed bio-oil phase containing <1% water and the catalyzed bio-oil containing approximately 2%, values that are statistically significantly different ($p < 0.05$). However, given the aqueous reaction media and different polarities and solubilities of the different biocrude components, we would not expect the water content of the bio-oil phases to be the same for both processes; the water present in the pyrolysis bio-oil was a product of the pyrolysis process. We could not distinguish whether water in the organic HTC phase was the result of the wet pyrolysis or present due to the incorporation of the aqueous reaction medium.

Table 1. Distribution of compound species detected in the GC-MS analysis of bio-oils derived from pyrolysis and HTC of avocado pits and avocado pits + bentonite. The reported values represent the percentage of each compound type out of the detectable compounds in the bio-oil. The average of two data points and the data range are presented. Total concentrations of detectable compounds ranged 30,000–50,000 mg compound/kg biomass.

Compound	Pyrolysis @ 600 °C		HTC @ 250 °C	
	Avocado	Avocado + Bentonite Clay	Avocado	Avocado + Bentonite Clay
	Percent (%) Compound Type			
Alcohols Data Range (%)	7.63% 5.27–9.99	8.86% 7.23–10.48		
Aldehydes Data Range (%)		3.75% 1.92–5.58		
Alkanes Data Range (%)	0.96% 0.00–1.92	0.47% 0.28–0.66		
Alkenes Data Range (%)		0.52% 0.35–0.68		
Esters Data Range (%)	0.29% 0.26–0.32	0.39% 0.30–0.49		
Furans Data Range (%)	28.35% 25.56–31.13	19.74% 13.45–26.03	100.00% -	33.74% 31.56–35.92
Ketones Data Range (%)	20.09% 17.86–22.32	18.88% 15.83–21.93		66.26% 64.08–68.44
Phenols Data Range (%)	29.84% 21.36–38.31	45.52% 31.27–59.78		
Oxygenated Aromatics Data Range (%)	6.56% 6.47–6.65	1.63% 0.00–3.27		
Others Data Range (%)		0.24% 0.00–0.48		

Throughout the literature, we see that during pyrolysis, lignin and cellulose undergo the greatest mass loss at 600 °C [41]; hence, we elected to hold the avocado pits at 600 °C for one hour to maximize bio-oil yields. During HTC, lignocellulosic material can degrade at much lower temperatures because of the drastic decrease in the water's dielectric constant as the pressure and temperature of the system approach the critical point. This makes water act as both an organic solvent and catalyst for degradation reactions such as decarbonylation and decarboxylation. This is an ideal system for high-moisture feedstocks, but as avocado pits (and bentonite clay) are dry materials, the peak reactivity was perhaps not reached

at the 250 °C reaction temperature. For both processes, the incorporation of clay was not expected to significantly lower the peak reactivity of the biomass but rather catalyze reactions that occur during pyrolysis/HTC, such as decarbonylation and decarboxylation as well as Diels–Adler, to improve the quality of the bio-oil.

The bio-oil obtained from HTC for both the biomass and biomass + clay mixture was furan and alcohol-based, and the incorporation of clay introduced a ketone, most probably resulting from the oxidation of a secondary alcohol [42].

The pyrolysis bio-oil derived from pure biomass consisted mainly of furans (28.35%), ketones (20.09%), alcohols (7.63%), and phenols (29.84%). The addition of clay to the pyrolysis feedstock shifted the distribution to furans (19.74%), ketones (18.88%), alcohols (8.86%), and phenols (42.52%), and it introduced aldehydes into the bio-oil. The production of aldehydes could be due to the oxidation of primary alcohols promoted by ionic groups present in the bentonite clay [42]. Fe, Si, and Al cations found in clay are reported in the literature as being responsible for promoting oxidation [43].

Gas chromatograms of biofuel analysis are presented in Figure S1. The addition of clay influenced the compounds present at higher retention times in the avocado pit bio-oil, which did not appear in the in situ upgraded bio-oil. This is notable as compounds detected at lower retention times have lower molecular weights than compounds detected at higher retention times due to the fact of their ability to move through the GC-MS column faster based on the polarity of the column and the compounds' size and geometry. By producing smaller compounds via catalytic reactions that breaks down larger compounds, the relative value of the bio-oil increases as a liquid fuel product [44].

Figure 1 shows the oxygen-to-carbon (O/C) ratios of the bio-oil as calculated by the oxygen and carbon content in the detected compounds. As mentioned, the bio-oil composition, presented in Table 1, represents compounds detectable by GC-MS. Decreased oxygen content, measured by the O/C ratio, is necessary to achieve a high-quality bio-oil for use as a liquid fuel. The O/C ratios typically range from 0.1 to 1.0 [45]. A decrease in oxygen functional groups is necessary for reduced acidity and viscosity and increased stability [46]. For both pyrolysis and HTC, the clay appeared to catalyze deoxygenation, ultimately lowering the O/C ratios of the bio-oil. As seen in Figure 1, it appeared that the incorporation of bentonite clay during pyrolysis decreased the O/C ratio from 0.60 to 0.40; however, due to the large deviation around the mean, the difference was not statistically significant, ($p > 0.05$). Bio-oil resulting from HTC had an O/C ratio decrease from 0.73 to 0.35, with a statistically significant difference between the samples ($p < 0.05$). This value corresponded only to compounds in the bio-oil, as it allows for a direct comparison between the pyrolysis and HTC bio-oils. It is notable, here, that the bio-oil produced from HTC was only a small fraction of the total recovered liquid from HTC. Should the carbonization temperature increase towards hydrothermal liquefaction temperatures (>250 °C) and the bio-oil content increase, the O/C ratio may decrease as more oxygen is shifted to the gas phase in the production of CO₂.

It is likely that the O/C ratio was reduced by deoxygenation at the catalytically active sites of the clay, specifically iron, which naturally occurs in bentonite clay [47] and has been reported to influence the formation of smaller molecules than those present in noncatalyzed bio-oil [48,49]. The mechanisms driving the formation of bio-oils during pyrolysis most commonly include catalytic cracking and hydrodeoxygenation. Catalytic cracking, which involves the fragmentation of large molecules into smaller compounds, removes oxygen via carbon monoxide and dioxide gases and water [50]. Hydrodeoxygenation removes oxygen through the loss of water, by sequential hydrogenation and dehydrogenation reactions [46]. The gas data in Figure 2 show that the carbon dioxide devolatilized during pyrolysis was lower for catalyzed pyrolysis, but water yields were increased for in situ catalyzed pyrolysis. As both samples underwent a drying phase at 110 °C for 30 min before reaching pyrolysis temperatures, the water peak at approximately 200 min was due to reactions, including hydrogenation and hydrogenolysis of C–O bonds, coupled with dehydration, which ultimately removed oxygen from the bio-oil to lower the O/C ratios [51].

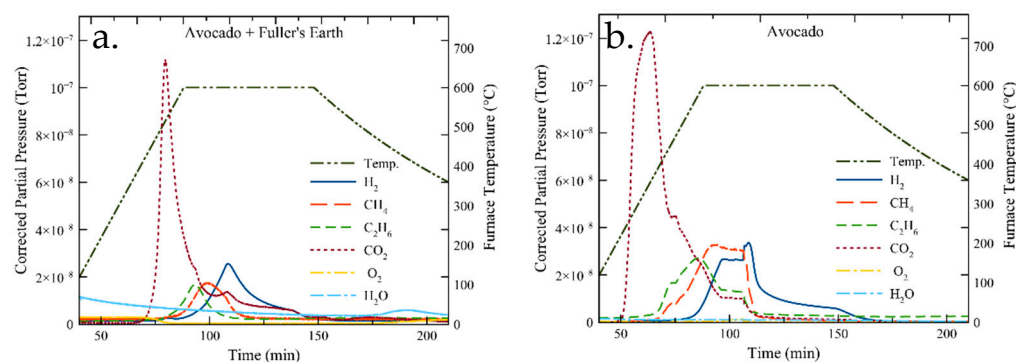


Figure 2. Gas emissions from pyrolysis of (a) avocado pits with 20% bentonite clay and (b) avocado pits.

At the catalyst active sites, lignin and cellulose produced anhydro-sugars that ultimately rearranged to form furan compounds [50], which accounted for 28% and 19% of the noncatalyzed and in situ catalyzed pyrolysis bio-oils, respectively. The decrease in furans in the catalyzed bio-oil may be due to the synergistic increase in phenol formation caused by catalytic cracking. The phenol content increased from 30% to 45% in the bio-oil when the clay was added to the pyrolysis feedstock; thus, while some C–C and O–C cracking occurred with no catalyst, the clay likely increased the cracking reactions as explained by Wan et al. [52].

During HTC, the mechanisms driving the transformation of biomass and production of bio-oil largely include hydrolysis and dehydration reactions [40]. Avocado pits have approximately 8% cellulose, 20% hemicellulose, and 13% lignin, while the rest consists of mainly fibers [53], which indicates that the bio-oil should consist mostly of cellulosic and hemicellulosic-derived products such as furans and small acids [40]. Tables S1 and S2 show the bio-oil and process water content, respectively. In the HTC bio-oil, furans were the majority of the detectable compounds. 5-Methylfurfural was detected with concentrations nearly identical to the HTC bio-oil with and without bentonite. 3-Furanmethanol was detected for both samples, with avocado pits + clay sample having a much lower concentration than only the hydrothermally carbonized avocado pits.

Cellulose undergoes hydrolysis and depolymerization reactions to form glucose, which then undergoes hydration and dehydration reactions to form furan-based compounds. In the bio-oils derived from HTC, the compounds detected included 3-furanmethanol, 1-2-furanyl-ethanone, 5-methylfurfural, and 2-methyl-2-cyclopenten-1-one. The decrease in furan concentrations indicate that furan groups may undergo Diels–Alder reactions in which the five-member aromatic furans react with olefins to ultimately form six-carbon aromatic groups, lowering the oxygen content of the bio-oil [54]. The process water contained only 2-5H-furanone for avocado pit-only carbonization and formic and propionic acids for avocado pit + clay carbonization as determined via HPLC (Figure 3). This indicates that with bentonite clay, furan groups were more likely to degrade to smaller organic acids via oxidation and hydration/dehydration reactions [40]. The supercritical water conditions of the HTC reaction provide an environment for oxidation to occur and ultimately produce small organic acids such as acetic, lactic, and formic acid from furans and carboxylic acids [40]. Both the process water and bio-oil showed that with the addition of bentonite clay to the feedstock, furans begin to break down into smaller compounds that were not present in the avocado pit-only samples.

Overall, bentonite promoted deoxygenation reactions during both processes for the resulting liquid products. Partial pressure gas emissions from pyrolysis of avocado pit and avocado pit + clay mixtures presented in Figure 2 show that the clay reduced hydrogen, methane, ethylene, and carbon dioxide production. Reduced emissions of noncondensable gases decreased the environmental impact of pyrolysis of the waste biomass for processes where bio-oil and biochar generation were prioritized.

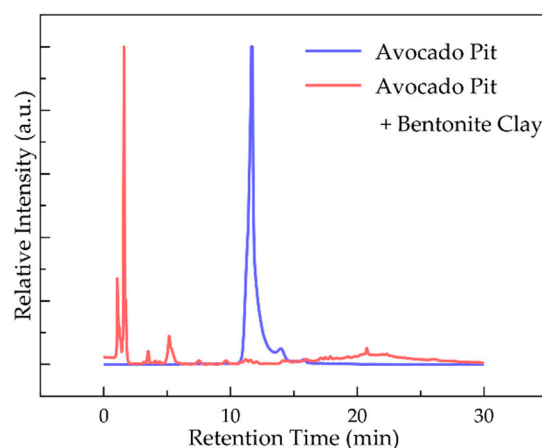


Figure 3. HPLC chromatogram from the HTC process water with avocado pits only and avocado pits + bentonite clay. Concentration of detected compounds are listed in Table S2.

2.2. Characterization of Bio- and Hydrochar

A proximate analysis was conducted via thermogravimetric analysis and the volatile matter, fixed carbon (FC), and ash contents are presented in Figure 4a. Results are presented on a dry basis. Pyrolysis and HTC with in situ catalyst resulted in chars with increased FC relative to the raw avocado pits, while VM decreased. The increase in FC and corresponding decrease in VM indicates that the chars are more stable relative to the raw biomass, and the chars may have applications as a soil amendment or water treatment material. In addition, the inclusion of the bentonite clay increased the solid yield for both processes from 31 to 35% and from 2 to 6% for pyrolysis and HTC, respectively (Figure 1). As was anticipated, bentonite clay has a high ash/mineral content and low volatile matter as it is composed primarily of inorganic smectite minerals, mostly montmorillonite (MMT, 80–90% by weight, full thermal stability provided in Figure S2). In contrast, the raw avocado pits are composed primarily of volatile matter as is typical of biomass.

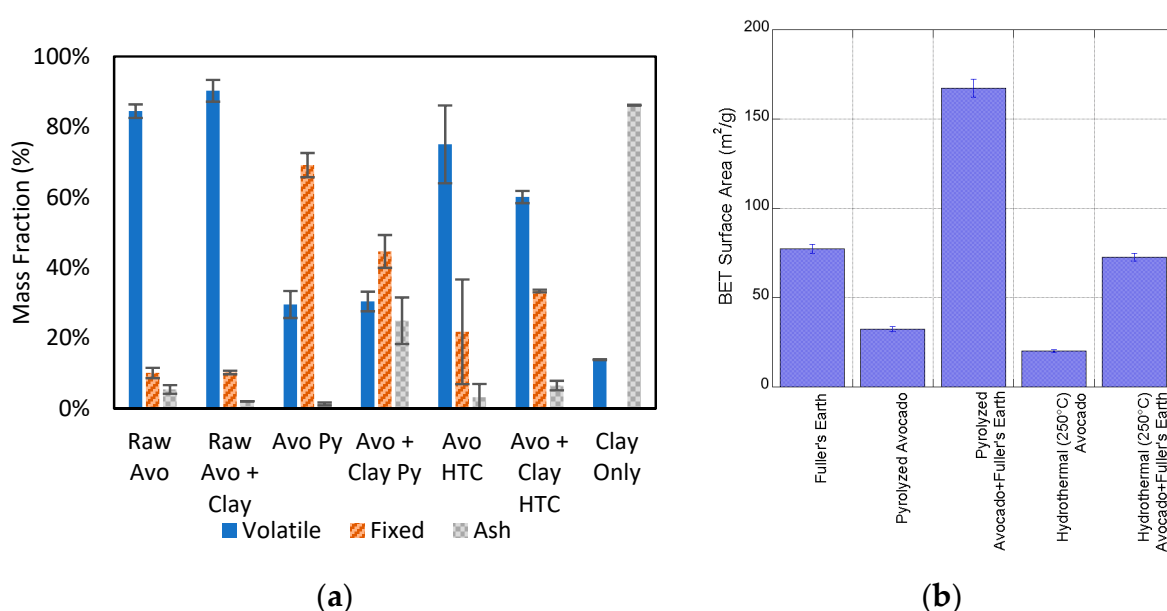


Figure 4. Characterization of raw materials, biochars, and hydrochars (error bars indicate one standard deviation) including (a) proximate analysis results (clay-free basis) and (b) surface area.

BET surface areas, as measured by N₂-Physisorption, are provided in Figure 4b. The incorporation of clay increases the BET surface area of both biochar and hydrochar and appears to promote the generation of a more porous network in the form of micropores and

surface structures. The effect of the bentonite clay on the structure of the chars is seen in the SEM images (Figure 5). The heterogeneous avocado pit + clay biochar mixture had the highest surface area ($167 \text{ m}^2/\text{g}$), while avocado biochar had a surface area of $34 \text{ m}^2/\text{g}$. The avocado pit biochar (Figure 5a) had a uniform macroporous structure, while the biochar formed in the presence of the clay had irregular porous structures (Figure 5b). The biochar made with clay had macroporous and microporous regimes that resulted in increased BET surface areas. The avocado pit hydrochar exhibited wide pores without a much visible microstructure on the surface of the char (Figure 5c). In contrast, the hydrochar produced with clay had an irregular microporous surface (Figure 5d). The increase in the surface area of the mixtures was unlikely due to the surface area contribution of the clay alone, whose BET surface area was measured at $77 \text{ m}^2/\text{g}$ [14]. The biomass to clay ratio was 5:1, but the surface areas of the biochar increased by more than 20%. By adding clay to HTC, the FC appeared to increase and the VM decrease, with little change in the ash content. This devolatilization promoted by the bentonite clay could result in the widening of the porous network and, therefore, explain the increase in the BET surface area. It is evident in the SEM images that there was an increase in micropores ($<2 \text{ nm}$) while maintaining the mesopores (2–50 nm) on the surface of the chars. The promotion of devolatilization was potentially a combination of the clay improving the heat transfer within the solid matrix, as the bentonite clay has a higher specific heat capacity than biomass [55] and possible oxygenated groups on the bentonite clay devolatilizing and partially oxidizing the char. The clay was not observed to block pores or form aggregates with the chars; a representative SEM image for the clay is provided in Figure S3. Overall, the clays appeared to promote devolatilization and the formation of micropores in the char increasing the surface area.

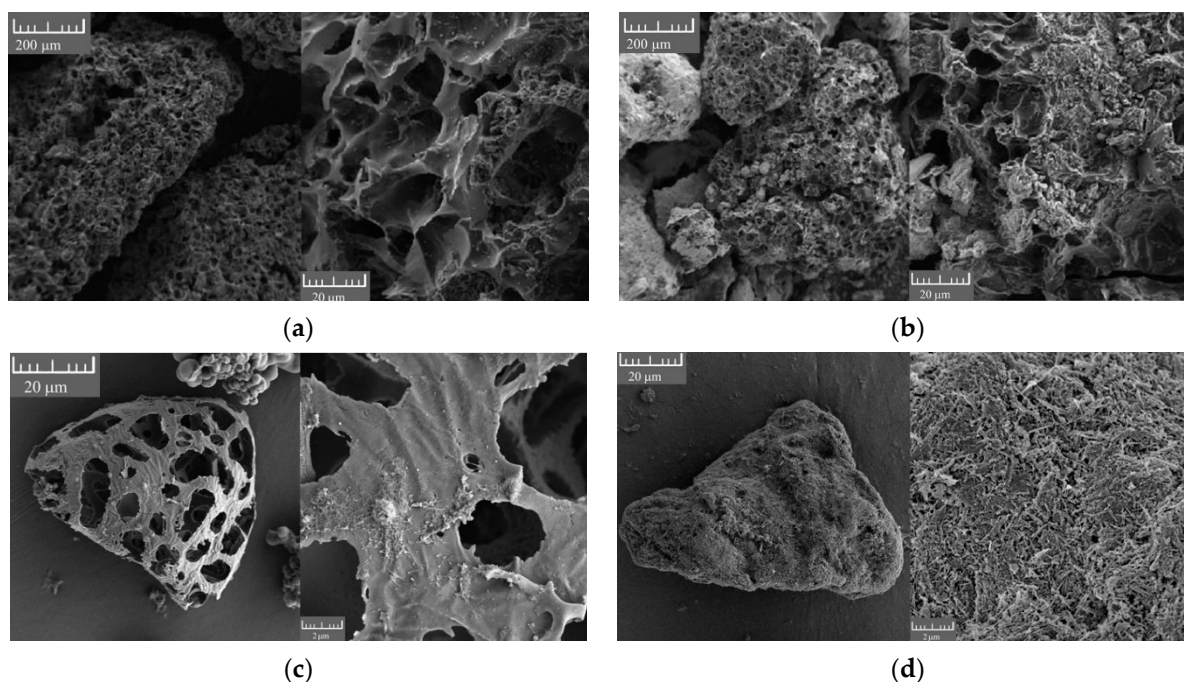


Figure 5. SEM images of pyrolyzed and hydrothermally carbonized avocado pits with and without the addition of 20 wt% Fuller's Earth: (a) avocado pyrolyzed at $600 \text{ }^\circ\text{C}$ (scale bar left image = $200 \text{ }\mu\text{m}$, right image = $20 \text{ }\mu\text{m}$); (b) avocado + Fuller's Earth pyrolyzed at $600 \text{ }^\circ\text{C}$ (scale bar left image = $200 \text{ }\mu\text{m}$, right image = $20 \text{ }\mu\text{m}$); (c) avocado hydrothermally carbonized at $250 \text{ }^\circ\text{C}$ (scale bar left image = $20 \text{ }\mu\text{m}$, right image = μm); (d) avocado + Fuller's Earth hydrothermally carbonized at $250 \text{ }^\circ\text{C}$ (scale bar left image = $20 \text{ }\mu\text{m}$, right image = $2 \text{ }\mu\text{m}$).

2.3. Summary: Impact of Bentonite on Pyrolysis and Hydrothermal Carbonization

In this work, we provide a side-by-side comparison of pyrolysis and HTC for the conversion of avocado pits with in situ clay catalysis. The incorporation of 20 wt% bentonite

clay during the thermochemical conversion process generated two value-added products, a biofuel, and a heterogeneous char. A summary of the impact of bentonite clay on both processes is included in Figure 6. For both processes, the clay decreased the O/C ratio of the bio-oils by catalyzing deoxygenation reactions, resulting in reduced acidity and viscosity and increased stability. The bio-oil contained furans and phenols, which have value as fuel precursors [56] as well as bioplastic precursors [57]. The incorporation of bentonite clay increases the solid yields for both thermochemical processes with the highest solid yield resulting from the pyrolysis of the avocado pit and clay mixture. The in situ catalyzed biochar also had the highest surface area. The noncondensable gas emissions during pyrolysis and gas yield from HTC both decrease with the incorporation of the clay catalyst. Providing this side-by-side comparison of two thermochemical processes, pyrolysis and HTC, is one of few in the existing literature to use the same biomass with an in situ catalyst and analyze the resulting char and bio-oils with a number of analytical techniques and instrumentation to understand how heating biomass in an inert environment, compared to a high-pressure wet environment, affects the structure of the biomass and composition of the bio-oil.

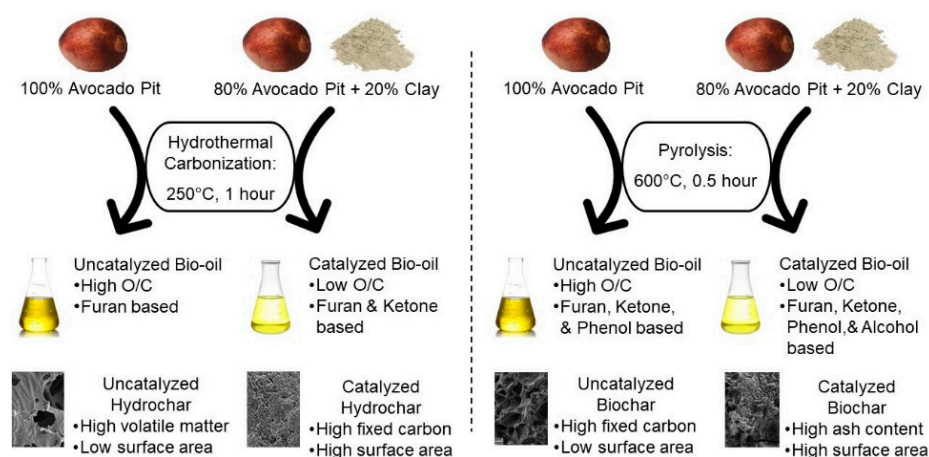


Figure 6. Summary of the thermochemical conversion processes and resulting product characteristics.

3. Materials and Methods

3.1. Materials

One dozen Haas avocados (*Persea americana*) were purchased at local grocery stores on four separate trips over three months to ensure a representative sample. The avocado pits were dried in an oven at 75 °C for 48 h and then mechanically ground and sieved into particle size fractions of 150–300 µm.

The bentonite clay (Fuller's Earth; sodium montmorillonite) was purchased from Fisher Scientific (Hampton, NH, USA) as a solid powder with particles less than 50 µm. To make the biomass–clay blend, 4.00 g of bentonite clay was added to 20.00 g of ground avocado pits (for a 20 wt% mixture, 5:1) in a clean beaker. The mixture was suspended in water (100.0 mL) for 30 min, then filtered and dried in a laboratory oven at 75 °C for 24 h to ensure consistent mixing. The pure avocado biomass was also suspended in water for the same time and similarly dried.

3.2. Pyrolytic Conversion of Biomass

Approximately 2.0 g of the sample was loaded into a porcelain boat in a 2'' MTI tube furnace. Samples were heated in 100 mL/min flowing high-purity nitrogen at a rate of 10 °C/min to 600 °C and held for 0.5 h. During the heating and hold time, the evolving gases were monitored using a Quadrupole Mass Spectrometer (Extorr XT Series RGA XT300M, New Kensington, PA, USA) studying AMU signals of 2, 16, 26, 27, 30, and 44 (H₂, CH₄, C₂H₂, C₂H₄, C₂H₆, and CO₂, respectively) (for more information on the use of these amu to monitor pyrolysis gas compounds, we refer the reader to Evans and

Milne [58] and Huang et al. [59]). The bio-oil components were condensed into 10 mL dichloromethane (DCM) (Acros Organics, HPLC grade) in glass cold traps for analysis. Following pyrolysis, the solid samples were cooled to room temperature under flowing nitrogen gas to prevent oxidation.

3.3. Hydrothermal Conversion of Biomass

Biomass (avocado pits) and the biomass + clay (avocado pits and bentonite clay) mixture were hydrothermally carbonized in a 300 mL stainless-steel batch reactor (Parr Instruments, Moline, IL, USA) with the same total mass of both samples. For hydrothermal carbonization of biomass, 10.0 g of sample was mixed with 150 mL of deionized water and heated to a temperature of 250 °C and a pressure of 4 MPa and held for 1 h under constant stirring at 150 rpm. For the biomass + clay sample, the process was also conducted in the same reactor. Previous studies have shown that at temperatures at or below 250 °C, the biomass-to-water (B/W) ratio in the process has a significant impact on the yield of products; here, an optimal ratio was selected from the literature [60].

The reactor was heated to 250 °C and reached an autogenous pressure of approximately 4 MPa and held for 1 h after reaching the set temperature under constant stirring at 150 rpm. The reactor was cooled to 20 °C and to final pressures of 0.8 and 0.7 MPa for the biomass and clay-biomass mixture, respectively. The hydrochar and HTC liquid were separated via vacuum filtration. The char was washed with 30 mL of methanol and dried in an oven overnight at 104 °C. 20 mL of the aqueous filtrate was contacted with 20 mL of n-hexane (Fisher Chemicals, HPLC grade) in a glass vial on a shaker table at 150 rpm for 24 h to extract the condensable bio-oil components. A 100 µL aliquot of the hexane layer was added to 1 mL of DCM in a glass vial and stored at 4 °C for subsequent analysis.

3.4. Analysis of Condensable Bio-Oils and Liquid Phase of HTC

The pyrolysis bio-oil was extracted from cold traps with 10.0 mL of DCM and analyzed on a GC 2010 Plus GC-MS (Shimadzu, Kyoto, Japan) with a cross-bond 30 m long 0.25 mm ID silica column. The GC oven was heated to 40 °C and the sample was then injected at 250 °C. The oven then was held at 40 °C for 5 min and ramped at 5 °C/min to 150 °C and held for an additional 5 min. The column was heated at 1.75 °C/min to 250 °C and held for 10 min. A 6-min solvent delay was used for the MS after which it was set to scan mode from 2 to 300 amu. The 6-min solvent delay is due to the solvent peak occurring at approximately 6 min. Any compounds that elute before this are indistinguishable from the solvent peak, limiting the detection of volatile compounds. Semiquantitative analysis was also performed by integrating the largest (by area) 50 peaks, with the GC-MS calibrated for several “marker” compounds. Water content of the bio-oil was determined via water extraction with anhydrous magnesium sulfate (AMS; Fisher Scientific). To obtain water content, approximately 1.0 g of bio-oil was added to a microcentrifuge tube containing 2.0 g of AMS. The tube was manually shaken and then centrifuged at 600 rpm for 5 min. The supernatant was then removed, and the tube was left open to dry overnight. After drying, the tube was measured to constant weight to determine the amount of water trapped in the AMS.

The composition of the aqueous phase of the HTC products was investigated using High-Performance Liquid Chromatography (HPLC, Shimadzu, Kyoto, Japan) with an Ultra Aqueous C18 Column. The column temperature was maintained at 25 °C at a total flow rate of 1.5 mL/min. The mobile phase consists of 10 mM phosphoric acid buffer solution (solvent A) and acetonitrile (solvent B) with a gradient condition of 90/10 (by volume) of A/B in the first 10 min, and 70/30 (by volume) of A/B from 10 to 50 min. The injection volume was 10 µL, and the detection wavelength was set at 210 nm.

3.5. Characterization of the Resulting Biochars and Hydrochars

The resulting biochars and hydrochars were extracted from the furnace and batch reactor, respectively, the clay catalyst remains in the solid phase after conversion. The prox-

imate analysis of the chars was performed using a TGA-DSC-1 (Mettler Toledo, Columbus, OH, USA). Proximate analysis of the clay-only sample was performed using a SDT-TGA 650 (TA Instruments, New Castle, DE, USA), using the same method of analysis. Between 5 and 12 mg of sample was placed in a 70 μ L alumina crucible and heated at 5 $^{\circ}$ C/min under high-purity nitrogen at 50 mL/min (with an additional 20 mL/min balance protective gas) from 25 to 110 $^{\circ}$ C and held at 110 $^{\circ}$ C for 0.5 h to remove moisture. Samples were further heated at 5 $^{\circ}$ C/min to 900 $^{\circ}$ C and held for 0.5 h; the total mass loss from 110 $^{\circ}$ C through the 900 $^{\circ}$ C hold was taken as volatile matter. Following this, the sample was heated in air at 50 mL/min to 950 $^{\circ}$ C and held for 0.5 h; the mass loss in this segment was attributed to fixed carbon. Residual mass was taken as the mineral matter/ash content. Measurements were performed in triplicate and the average and standard deviation are reported.

The surface area of the samples was measured using N_2 -physisorption isotherms on a Autosorb-iQ (Quantachrome, Boynton Beach, FL, USA). Samples were degassed at 180 $^{\circ}$ C for a minimum of 16 h. Data were analyzed using the Brunauer–Emmett–Teller (BET) adsorption method over a partial pressure range of 0.05 to 0.3.

Scanning electron microscopy (SEM) images were conducted on the uncoated biochars and hydrochars using a Mira3 field-emission scanning electron microscope (Tescan, Brno, Czechia) with an accelerating voltage of 5 kV.

Supplementary Materials: The following supporting information can be downloaded at: <https://www.mdpi.com/article/10.3390/catal12060655/s1>, Table S1: Complete compound species breakdown for bio-oils as detected by GC-MS; Figure S1: Gas chromatograms of biofuel analysis; Table S2: HP-LC analysis of aqueous product from hydrothermal carbonization; Table S3: Water content of pyrolysis bio-oil; Table S4: Pyrolysis and HTC yields and O/C ratios; Figure S2: Thermal stability curve for bentonite clay; Figure S3: SEM image of bentonite clay.

Author Contributions: Conceptualization, J.L.G. and G.D.; methodology, G.D. and L.G.; investigation, M.K., M.T.A., L.G. and Z.A.P.; resources, J.L.G.; data analysis, M.K., M.T.A. and Z.A.P.; writing—original draft preparation, M.K. and M.T.A.; writing—review and editing, J.L.G. and Z.A.P.; supervision, J.L.G.; project administration, J.L.G.; funding acquisition, G.D. and J.L.G. All authors have read and agreed to the published version of the manuscript.

Funding: G.D. acknowledges support from the China Scholarship Council (CSC) under Grant CSC NO. 201506425012. This work was partially funded by the US National Science Foundation, under grant numbers 1727316 and 2031916, and by a Hatch Grant, under accession number 1021398, from the USDA National Institute of Food and Agriculture. This work made use of the Cornell Center for Materials Research Facilities supported by the National Science Foundation under Award Number DMR-1719875.

Data Availability Statement: Raw data are available from the corresponding author upon request.

Conflicts of Interest: The authors declare no conflict of interest.

References

1. Ruhul Kabir, M.; Kumar, A. Comparison of the energy and environmental performances of nine biomass/coal co-firing pathways. *Bioresour. Technol.* **2012**, *124*, 394–405. [[CrossRef](#)] [[PubMed](#)]
2. United Nations. Goal 14 | Department of Economic and Social Affairs. Available online: <https://sdgs.un.org/goals/goal14> (accessed on 7 June 2022).
3. Pham, T.N.; Shi, D.; Resasco, D.E. Environmental Evaluating strategies for catalytic upgrading of pyrolysis oil in liquid phase. *Appl. Catal. B Environ.* **2014**, *145*, 10–23. [[CrossRef](#)]
4. Mante, O.D.; Agblevor, F.A. Catalytic pyrolysis for the production of refinery-ready biocrude oils from six different biomass sources. *Green Chem.* **2014**, *16*, 3364. [[CrossRef](#)]
5. Alonso, D.M.; Bond, J.Q.; Dumesic, J.A. Catalytic conversion of biomass to biofuels. *Green Chem.* **2010**, *12*, 1493–1513. [[CrossRef](#)]
6. Yogalakshmi, K.N.; Poornima, D.T.; Sivashanmugam, P.; Kavitha, S.; Yukesh, K.R.; Varjani, S.; AdishKumar, S.; Kumar, G.; Banu, R.J. Lignocellulosic biomass-based pyrolysis: A comprehensive review. *Chemosphere* **2022**, *286*, 131824. [[CrossRef](#)]
7. Lyu, G.; Wu, S.; Zhang, H. Estimation and Comparison of Bio-Oil Components from Different Pyrolysis Conditions. *Front. Energy Res.* **2015**, *3*, 28. [[CrossRef](#)]
8. Feng, J.; Yang, Z.; Hse, C.; Su, Q.; Wang, K.; Jiang, J.; Xu, J. In situ catalytic hydrogenation of model compounds and biomass-derived phenolic compounds for bio-oil upgrading. *Renew. Energy* **2017**, *105*, 140–148. [[CrossRef](#)]

9. He, J.; Kunitake, T.; Nakao, A. Facile In Situ Synthesis of Noble Metal Nanoparticles in Porous Cellulose Fibers. *Chem. Mater.* **2003**, *15*, 4401–4406. [[CrossRef](#)]
10. Iliopoulou, E.; Stefanidis, S.; Kalogiannis, K. Catalytic upgrading of biomass pyrolysis vapors using transition metal-modified ZSM-5 zeolite. *Appl. Catal. B* **2012**, *127*, 281–290. [[CrossRef](#)]
11. Gökdağ, Z.; Sinağ, A.; Yumak, T. Comparison of the catalytic efficiency of synthesized nano tin oxide particles and various catalysts for the pyrolysis of hazelnut shell. *Biomass Bioenergy* **2010**, *34*, 402–410. [[CrossRef](#)]
12. Li, J.; Yan, R.; Xiao, B.; Liang, D.; Lee, D. Preparation of Nano-NiO Particles and Evaluation of Their Catalytic Activity in Pyrolyzing Biomass Components†. *Energy Fuels* **2007**, *333*, 16–23. [[CrossRef](#)]
13. Ischia, M.; Maschio, R.D.; Grigiante, M.; Baratieri, M. Clay-sewage sludge co-pyrolysis. A TG-MS and Py-GC study on potential advantages afforded by the presence of clay in the pyrolysis of wastewater sewage sludge. *Waste Manag.* **2011**, *31*, 71–77. [[CrossRef](#)] [[PubMed](#)]
14. Dou, G.; Goldfarb, J.J.L. In situ upgrading of pyrolysis biofuels by bentonite clay with simultaneous production of heterogeneous adsorbents for water treatment. *Fuel* **2017**, *195*, 273–283. [[CrossRef](#)]
15. De Resende, E.C.; Gissane, C.; Nicol, R.; Heck, R.J.; Guerreiro, M.C.; Coelho, J.V.; De Oliveira, L.C.A.; Palmisano, P.; Berruti, F.; Briens, C.; et al. Synergistic co-processing of Red Mud waste from the Bayer process and a crude untreated waste stream from bio-diesel production. *Green Chem.* **2013**, *15*, 496. [[CrossRef](#)]
16. Ooi, X.Y.; Gao, W.; Ong, H.C.; Lee, H.V.; Juan, J.C.; Chen, W.H.; Lee, K.T. Overview on catalytic deoxygenation for biofuel synthesis using metal oxide supported catalysts. *Renew. Sustain. Energy Rev.* **2019**, *112*, 834–852. [[CrossRef](#)]
17. Oi, L.E.; Choo, M.Y.; Lee, H.V.; Ong, H.C.; Hamid, S.B.A.; Juan, J.C. Recent advances of titanium dioxide (TiO₂) for green organic synthesis. *RSC Adv.* **2016**, *6*, 108741–108754. [[CrossRef](#)]
18. Wu, L.M.; Zhou, C.H.; Tong, D.S.; Yu, W.H.; Wang, H. Novel hydrothermal carbonization of cellulose catalyzed by montmorillonite to produce kerogen-like hydrochar. *Cellulose* **2014**, *21*, 2845–2857. [[CrossRef](#)]
19. Cheng, F.; Tompsett, G.A.; Murphy, C.M.; Maag, A.R.; Carabillo, N.; Bailey, M.; Hemingway, J.J.; Romo, C.I.; Paulsen, A.D.; Yelvington, P.E.; et al. Synergistic Effects of Inexpensive Mixed Metal Oxides for Catalytic Hydrothermal Liquefaction of Food Wastes. *ACS Sustain. Chem. Eng.* **2020**, *8*, 6877–6886. [[CrossRef](#)]
20. Ma, Q.; Wang, K.; Sudibyo, H.; Tester, J.W.; Huang, G.; Han, L.; Goldfarb, J.L. Production of upgraded biocrude from hydrothermal liquefaction using clays as in situ catalysts. *Energy Convers. Manag.* **2021**, *247*, 114764. [[CrossRef](#)]
21. Rahman, T.; Jahromi, H.; Roy, P.; Adhikari, S.; Hassani, E.; Oh, T.S. Hydrothermal liquefaction of municipal sewage sludge: Effect of red mud catalyst in ethylene and inert ambiances. *Energy Convers. Manag.* **2021**, *245*, 114615. [[CrossRef](#)]
22. Maged, A.; Kharbish, S.; Ismael, I.S.; Bhatnagar, A. Characterization of activated bentonite clay mineral and the mechanisms underlying its sorption for ciprofloxacin from aqueous solution. *Environ. Sci. Pollut. Res. Int.* **2020**, *27*, 32980. [[CrossRef](#)] [[PubMed](#)]
23. Bu, H.; Yuan, P.; Liu, H.; Liu, D.; Liu, J.; He, H.; Zhou, J.; Song, H.; Li, Z. Effects of complexation between organic matter (OM) and clay mineral on OM pyrolysis. *Geochim. Cosmochim. Acta* **2017**, *212*, 1–15. [[CrossRef](#)]
24. Singhvi, M.S.; Gokhale, D.V. Lignocellulosic biomass: Hurdles and challenges in its valorization. *Appl. Microbiol. Biotechnol.* **2019**, *103*, 9305–9320. [[CrossRef](#)] [[PubMed](#)]
25. Işitan, S.; Ceylan, S.; Topcu, Y.; Hintz, C.; Tefft, J.; Chellappa, T.; Guo, J.; Goldfarb, J.L.; Istan, S.; Ceylan, S.; et al. Product quality optimization in an integrated biorefinery: Conversion of pistachio nutshell biomass to biofuels and activated biochars via pyrolysis. *Energy Convers. Manag.* **2016**, *127*, 576–588. [[CrossRef](#)]
26. Dehkhoda, A.M.; Gyenge, E.; Ellis, N. A novel method to tailor the porous structure of KOH-activated biochar and its application in capacitive deionization and energy storage. *Biomass Bioenergy* **2016**, *87*, 107–121. [[CrossRef](#)]
27. Linares-Solano, A.; Lillo-Ródenas, M. NaOH and KOH for preparing activated carbons used in energy and environmental applications. *J. Energy* **2012**, *20*, 59–91.
28. Gao, Y.; Yue, Q.; Gao, B.; Sun, Y.; Wang, W.; Li, Q.; Wang, Y. Comparisons of porous, surface chemistry and adsorption properties of carbon derived from *Enteromorpha prolifera* activated by H₄P₂O₇ and KOH. *Chem. Eng. J.* **2013**, *232*, 582–590. [[CrossRef](#)]
29. Tan, X.; Liu, S.; Liu, Y.; Gu, Y.; Zeng, G.; Hu, X.; Wang, X.; Liu, S.; Jiang, L. Biochar as potential sustainable precursors for activated carbon production: Multiple applications in environmental protection and energy storage. *Bioresour. Technol.* **2017**, *227*, 359–372. [[CrossRef](#)]
30. Goldfarb, J.L.; Buessing, L.; Gunn, E.; Lever, M.; Billias, A.; Casoliba, E.; Schievano, A.; Adani, F. Novel Integrated Biorefinery for Olive Mill Waste Management: Utilization of Secondary Waste for Water Treatment. *ACS Sustain. Chem. Eng.* **2017**, *5*, 876–884. [[CrossRef](#)]
31. Ramola, S.; Belwal, T.; Li, C.J.; Wang, Y.Y.; Lu, H.H.; Yang, S.M.; Zhou, C.H. Improved lead removal from aqueous solution using novel porous bentonite - and calcite-biochar composite. *Sci. Total Environ.* **2020**, *709*, 136171. [[CrossRef](#)]
32. Chen, L.; Chen, X.L.; Zhou, C.H.; Yang, H.M.; Ji, S.F.; Tong, D.S.; Zhong, Z.K.; Yu, W.H.; Chu, M.Q. Environmental-friendly montmorillonite-biochar composites: Facile production and tunable adsorption-release of ammonium and phosphate. *J. Clean. Prod.* **2017**, *156*, 648–659. [[CrossRef](#)]

33. Zelaya Soulé, M.E.; Fernández, M.A.; Montes, M.L.; Suárez-García, F.; Torres Sánchez, R.M.; Tascón, J.M.D. Montmorillonite-hydrothermal carbon nanocomposites: Synthesis, characterization and evaluation of pesticides retention for potential treatment of agricultural wastewater. *Colloids Surf. A Physicochem. Eng. Asp.* **2020**, *586*, 124192. [CrossRef]
34. Wu, X.; Gao, P.; Zhang, X.; Jin, G.; Xu, Y.; Wu, Y. Synthesis of clay/carbon adsorbent through hydrothermal carbonization of cellulose on palygorskite. *Appl. Clay Sci.* **2014**, *95*, 60–66. [CrossRef]
35. Sarkar, B.; Liu, E.; McClure, S.; Sundaramurthy, J.; Srinivasan, M.; Naidu, R. Biomass derived palygorskite-carbon nanocomposites: Synthesis, characterisation and affinity to dye compounds. *Appl. Clay Sci.* **2015**, *114*, 617–626. [CrossRef]
36. “Avocados”. Agricultural Marketing Resource Center, Iowa State University. Available online: <https://www.agmrc.org/commodities-products/fruits/avocados> (accessed on 7 June 2022).
37. Alvarez, F. “Here’s the Scoop on Guacamole”. Los Angeles Times. Available online: <https://www.latimes.com/archives/la-xpm-2001-dec-06-me-12000-story.html> (accessed on 7 June 2022).
38. Libra, J.A.; Ro, K.S.; Kammann, C.; Funke, A.; Berge, N.D.; Neubauer, Y.; Titirici, M.M.; Fühner, C.; Bens, O.; Kern, J.; et al. Hydrothermal carbonization of biomass residuals: A comparative review of the chemistry, processes and applications of wet and dry pyrolysis. *Biofuels* **2011**, *2*, 71–106. [CrossRef]
39. Sangaré, D.; Moscossa-Santillan, M.; Antonio, P.A.; Bostyn, S.; Belandria, V.; Gökalp, I. Hydrothermal carbonization of biomass: Experimental study, energy balance, process simulation, design, and techno-economic analysis. *Biomass Convers. Biorefin.* **2022**, *1–16*. [CrossRef]
40. Wüst, D.; Correa, C.R.; Jung, D.; Zimmermann, M.; Kruse, A.; Fiori, L. Understanding the influence of biomass particle size and reaction medium on the formation pathways of hydrochar. *Biomass Convers. Biorefin.* **2020**, *10*, 1357–1380. [CrossRef]
41. Hubble, A.H.; Goldfarb, J.L. Synergistic effects of biomass building blocks on pyrolysis gas and bio-oil formation. *J. Anal. Appl. Pyrolysis* **2021**, *156*, 105100. [CrossRef]
42. Loudon, M. Reduction of Aldehydes and Ketones to Alcohols. In *Organic Chemistry*; Pearson: London, UK, 2015; p. 926, ISBN 1936221349.
43. Carriazo, J.G.; Centeno, M.A.; Odriozola, J.A.; Moreno, S.; Molina, R. Effect of Fe and Ce on Al-pillared bentonite and their performance in catalytic oxidation reactions. *Appl. Catal. A Gen.* **2007**, *317*, 120–128. [CrossRef]
44. Hubble, A.H.; Ryan, E.M.; Goldfarb, J.L. Enhancing pyrolysis gas and bio-oil formation through transition metals as in situ catalysts. *Fuel* **2022**, *308*, 121900. [CrossRef]
45. Negahdar, L.; Gonzalez-Quiroga, A.; Otyuskaya, D.; Toraman, H.E.; Liu, L.; Jastrzebski, J.T.B.H.; Van Geem, K.M.; Marin, G.B.; Thybaut, J.W.; Weckhuysen, B.M. Characterization and Comparison of Fast Pyrolysis Bio-oils from Pinewood, Rapeseed Cake, and Wheat Straw Using ¹³C NMR and Comprehensive GC × GC. *ACS Sustain. Chem. Eng.* **2016**, *4*, 4974–4985. [CrossRef] [PubMed]
46. Palacio Lozano, D.C.; Jones, H.E.; Ramirez Reina, T.; Volpe, R.; Barrow, M.P. Unlocking the potential of biofuels via reaction pathways in van Krevelen diagrams. *Green Chem.* **2021**, *23*, 8949–8963. [CrossRef]
47. Komadel, P.; Anastácio, A.S.; Andrejkovičová, S.; Stucki, J.W. Iron phases identified in bentonite from the Lieskovec deposit (Slovakia) by variable-temperature Mössbauer spectroscopy. *Clay Miner.* **2008**, *43*, 107–115. [CrossRef]
48. Sulman, M.; Kosivtsov, Y.; Sulman, E.; Alfyorov, V.; Lugovoy, Y.; Molchanov, V.; Tyamina, I.; Misnikov, O.; Afanasjev, A.; Kumar, N.; et al. Influence of aluminosilicate materials on the peat low-temperature pyrolysis and gas formation. *Chem. Eng. J.* **2009**, *154*, 355–360. [CrossRef]
49. Ro, D.; Shafaghat, H.; Jang, S.H.; Lee, H.W.; Jung, S.C.; Jae, J.; Cha, J.S.; Park, Y.K. Production of an upgraded lignin-derived bio-oil using the clay catalysts of bentonite and olivine and the spent FCC in a bench-scale fixed bed pyrolyzer. *Environ. Res.* **2019**, *172*, 658–664. [CrossRef]
50. Rahman, M.M.; Liu, R.; Cai, J. Catalytic fast pyrolysis of biomass over zeolites for high quality bio-oil—A review. *Fuel Process. Technol.* **2018**, *180*, 32–46. [CrossRef]
51. Yan, L.; Zhang, Q.; Deng, W.; Zhang, Q.; Wang, Y. Catalytic valorization of biomass and bioplatfroms to chemicals through deoxygenation. *Adv. Catal.* **2020**, *66*, 1–108. [CrossRef]
52. Wan, Z.; Wang, S.; Li, Z.; Yi, W.; Zhang, A.; Li, Y.; Zhang, P. Co-pyrolysis of lignin and spent bleaching clay: Insight into the catalytic characteristic and hydrogen supply of spent bleaching clay. *J. Anal. Appl. Pyrolysis* **2022**, *163*, 105491. [CrossRef]
53. Barbosa-Martín, E.; Chel-Guerrero, L.; González-Mondragón, E.; Betancur-Ancona, D. Chemical and technological properties of avocado (*Persea americana* Mill.) seed fibrous residues. *Food Bioprod. Process.* **2016**, *100*, 457–463. [CrossRef]
54. Zuo, W.; Wong, H.-W. Green synthesis of linear alkylbenzenes via Diels–Alder cycloaddition between furan and linear alkenes over niobic acid catalyst. *Green Chem. Lett. Rev.* **2017**, *10*, 393–403. [CrossRef]
55. Cara, S.; Carcangiu, G.; Padalino, G.; Palomba, M.; Tamanini, M. The bentonites in pelotherapy: Thermal properties of ž/clay pastes from Sardinia Italy. *Appl. Clay Sci.* **2000**, *16*, 125–132. [CrossRef]
56. Westbrook, C.K.; Curran, H.J. Detailed kinetics of fossil and renewable fuel combustion. *Comput. Aided Chem. Eng.* **2019**, *45*, 363–443. [CrossRef]
57. Bello, S.; Méndez-Trelles, P.; Rodil, E.; Feijoo, G.; Moreira, M.T. Towards improving the sustainability of bioplastics: Process modelling and life cycle assessment of two separation routes for 2,5-furandicarboxylic acid. *Sep. Purif. Technol.* **2020**, *233*, 116056. [CrossRef]

-
58. Evans, R.J.; Milne, T.A. Molecular Characterization of the Pyrolysis of Biomass. 2. Applications. *Energy Fuels* **1987**, *1*, 311–319. [[CrossRef](#)]
 59. Huang, Y.F.; Kuan, W.H.; Chiueh, P.T.; Lo, S.L. Pyrolysis of biomass by thermal analysis–mass spectrometry (TA–MS). *Bioresour. Technol.* **2011**, *102*, 3527–3534. [[CrossRef](#)]
 60. Volpe, M.; Fiori, L. From olive waste to solid biofuel through hydrothermal carbonisation: The role of temperature and solid load on secondary char formation and hydrochar energy properties. *J. Anal. Appl. Pyrolysis* **2017**, *124*, 63–72. [[CrossRef](#)]